TECHNICAL PAPER

Investigation of the effect of ultrasonic micro-welding process parameters on the microstructure components bonding

Mehrzad Modarres[1,2] · Mohammad Tahmasebipour[1,2]

Abstract

In this paper, the application of the ultrasonic micro-welding process has been presented for bonding the microstructures. Two sheets made of the PMMA (including a micro-channel, inlet, and outlet) were connected by applying the ultrasonic waves with 20 kHz frequency and 2000-W power. The effects of the important parameters of the ultrasonic micro-welding process including energy directors (EDs) height (300, 450, and 600 micrometers), applied pressure (2, 2.5, and 3 bar) and time (0.1, 0.2, and 0.3 s) have been investigated on the distribution of the generated temperature during the ultrasonic welding process, affected areas by the ultrasonic welding as well as compressive-shear strength of the samples. In this study, the Taguchi method has been used to achieve the optimal levels of the mentioned parameters by analysis of the signal-to-noise (*S/N*) ratios, and the order of importance of the process parameters was specified by using the analysis of variance of the *S/N* ratios. The optimal levels of the parameters of the micro-welding process were determined as EDs height of 300 μm, applied pressure of 3 bar, and process time of 0.1 s. The amount of max. temperature, welding area, and max. compressive-shear strength obtained for optimal levels of the process parameters was assessed as 398 K, 15.17 mm^2, and 5.2e13 Pa, respectively.

Keywords Ultrasonic micro-welding · Micro-bonding · Microstructure · Micro-manufacturing · Micro-fabrication · PMMA · Taguchi · Analysis of variance · ANOVA

1 Introduction

Ultrasonic waves are a group of mechanical waves that their frequency exceeds the range of human hearing (20 to 20,000 Hz). These waves have various applications due to their properties. Welding is one of the most important and practical methods for bonding various parts. Nowadays, micro-electromechanical sensors [1–4] and actuators [5–7], and microfluidic systems [8] have found many applications in various industries. Development of the welding methods is very important for the production of the microsystems. Specifically, in fabrication of the microfluidic systems, the

bonding is an essential step for the sealing of micro-channels, micro-valves, micro-pumps, and micrometer chambers.

Common bonding methods in micro-electromechanical systems (MEMS) fabrication are including organic bonding [9], anodic bonding [10], fusion bonding [11], bonding via reactive metals [12], ultrasonic welding [13], and resistance welding [14]. Ultrasonic welding has received more attention than other connection methods because of no need for filler or additives materials. Also, slight heat zone and the cleanliness of the connection area. In addition, this method is used for welding and joining the microstructures by controlling applied forces to prevent them from deformation. Figure 1 shows a schematic form of an ultrasonic welding machine that is consisting of a power supply, force applying system, converter, amplifier or booster, and a tool for wave guidance that is called horn [15].

The ultrasonic metal welding process is fundamentally different from welding of the plastics in how the ultrasonic energy (or vibrations) is delivered to the weld, and in how the actual weld is created. First, the ultrasonic metal welding delivers vibrations to the welding zone via transverse vibrations that are parallel to the weld surfaces [16]. But,

✉ Mohammad Tahmasebipour
  tahmasebipour@ut.ac.ir

1 Faculty of New sciences and Technologies, University of Tehran, Tehran 1439957131, Iran

2 Micro/Nanofabrication Technologies Lab, Faculty of New Sciences and Technologies, University of Tehran, Tehran 1439957131, Iran
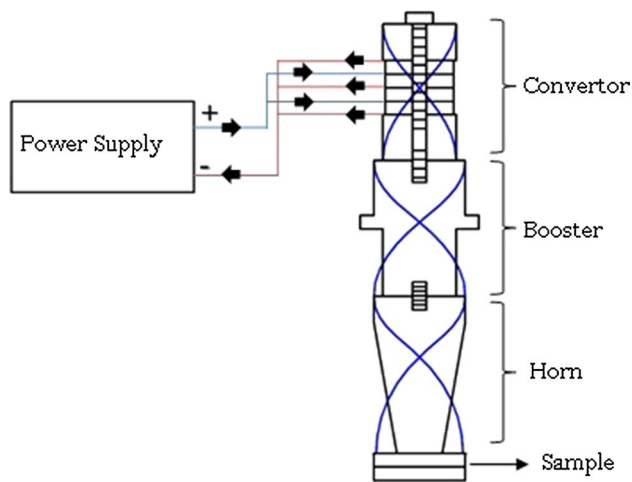
Fig. 1 Schematic form of an ultrasonic welding machine

Fig. 2 Geometrical form of the samples components, **a** top plate: EDs, inlet, and outlet and **b** bottom plate: micro-channel

ultrasonic plastic welding delivers vibrations to the zone via longitudinal vibrations that are normal to the weld surfaces (Fig. 1). Second, in the ultrasonic metal welding, temperature does not exceed the melting point of the welding materials. But, ultrasonic plastic welding is based on melting and fusion of the material.

By considering the appropriate conditions, ultrasonic welding can join the micrometer components to each other. Furthermore, assembling, sealing, and packaging of the micro-electromechanical and microfluidic systems can be performed using ultrasonic welding. Some of the most important research in this field are as follows:

Roman Truckenmuller et al. used the ultrasonic welding process to make micro-sensors, micro-pumps, and micro-actuators [17]. Chen et al. proposed the ultrasonic welding process to make carbon nanotube transistors [18]. Grund et al. used ultrasonic welding to bonding the connections to the micro-valves [19]. Min et al. offered an ultrasonic welding method to save proteins in micro-parts that has made of biodegradable polymers for drug delivery and implants [20]. Luo et al. proposed the ultrasonic welding method, along with heating the samples to connect PMMA microfluidic components [21]. Michaeli et al. used ultrasonic welding to the molding of the polymer micro-parts [22]. Van Oordt et al. used ultrasonic welding to package aluminum foils to maintain chemical solutions and reactors in the lab-on-a-chip (LOAC) systems [23]. According to the literature review, the ultrasonic micro-welding method has a high capacity for use in connecting micro-electromechanical components because of not using foreign materials, less heat zone, cleanliness of the connection zone, high quality of the welding, compatibility with the chemical and biological environments, no plastic deformation in the work-piece, high speed of the welding, ability to automate the process, the possibility of using in
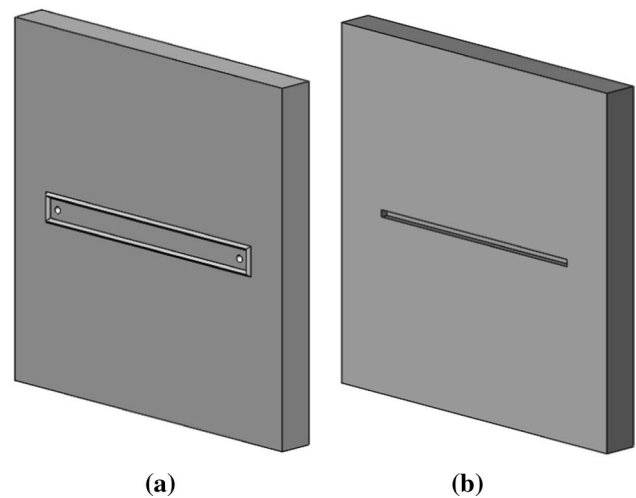
mass production, high mechanical strength, and the possibility of welding at room temperature.

In the present study, the finite element method is used to investigate the mechanical–thermal behavior of the ultrasonic micro-welded PMMA samples. These samples include a top plate (containing energy directors with different dimensions, and two micro-holes; micro-channel's inlet and outlet) and a bottom plate (containing a micro-channel) that are connected by the ultrasonic welding machine with 20 kHz frequency and 2000-W power. The effects of the important parameters of the ultrasonic micro-welding process including energy directors (EDs) height, applied pressure and time are investigated on the distribution of the generated temperature during the ultrasonic welding process, affected areas by the ultrasonic welding as well as compressive-shear strength of the samples. The Taguchi method is used to achieve the optimal levels of the mentioned parameters by analysis of the signal-to-noise (*S/N*) ratios and the order of importance of the process parameters is specified by using the analysis of variance (ANOVA) of the *S/N* ratios.

2 Materials and methods

In this research, fabrication of the components of the microstructure samples and their bonding using ultrasonic microwelding have been conducted. Then, COMSOL software has been used for simulating the ultrasonic micro-welding process using the finite element method (FEM). The geometric form of the microstructure components used in ultrasonic micro-welding is shown in Fig. 2. The top plate of the samples includes energy directors (EDs) with isosceles triangle cross section and two holes as inlet and outlet of the

micro-channel. On the bottom plate, a micro-channel with dimensions of 400 μm × 400 μm × 14 mm has been created.

Energy directors concentrate heat dissipation resulted from ultrasonic vibrations due to their low stiffness and high cyclic strain at the joint interface. The maximum friction and hysteresis losses phenomena occur in the EDs. Therefore, they can absorb the most amount of the ultrasonic waves that come from the horn (the horn shape is shown in Fig. 3). These waves result in heating up and melting the plastic. The higher the amount of EDs height the higher the friction, leading to the higher temperature. The high bonding strength of the welded joints can be attributed to the high temperature at the interface between the upper and lower sheets of the samples, which results in better melting and bonding.

The samples dimensions are shown in Fig. 4. The samples have been made of Poly-methyl methacrylate (PMMA) with the specifications given in Table 1. Microstructure components were fabricated using a precise CNC milling machine. SEM (Cam Scan-MV2300) picture and optical microscopic image of the microstructure components are shown in Fig. 5.

3 Design of experiments

In the ultrasonic micro-welding process, the components to be welded are held together under pressure and then subjected to a high-frequency oscillation. At this stage, under high-frequency and application of pressure, the temperature of energy directors increases by damping the oscillations up to the melting temperature of poly-methyl methacrylate (PMMA). After a certain period of time, the vibrations are turned off and the applied pressure decreases into the holding pressure. The melted EDs flow at the interface between the upper and lower sheets of the samples. After

Table 1 Characteristics of the PMMA material [24, 25]

Property	Value	Unit
Thermal conductivity	0.2	W/(m K)
Coefficient of thermal expansion	$70\,e^{-6}$	1/K
Density	1190	kg/m^3
Heat capacity at constant pressure	1300	J/(kg K)
Shear modulus	1700	N/m^2
Bulk modulus	$6\,e^9$	N/m^2

that, adhesion and entanglement of polymer chains occur across the interface, so the weld occurs. The ability to weld two components using ultrasonic welding depends on material properties, joint design, welding frequency, and welding time. The dimensions of EDs are very small in comparison with the whole dimensions of the microstructure. Therefore, deformation in the microstructure occurs in a small area that isn't comparable with the overall dimensions of the microstructure.

In this study, the Taguchi method was used to find the optimal process parameters for connecting two parts of the microstructure using ultrasonic micro-welding. Taguchi has presented a systematic method that efficiently selects the set of experiments from all possible combinations which is useful to optimize the output economically in terms of performance and quality [26, 27]. This approach uses a set of arrays called orthogonal arrays that denes the minimal number of experiments that could give the complete information of all the factors that affect the outcome. Each experiment's results are converted to a signal-to-noise (*S/N*) ratio to determine the combination of control factor levels to improve the system's stability and reduce quality loss [28]. Taguchi's method is an efficient and important optimization method

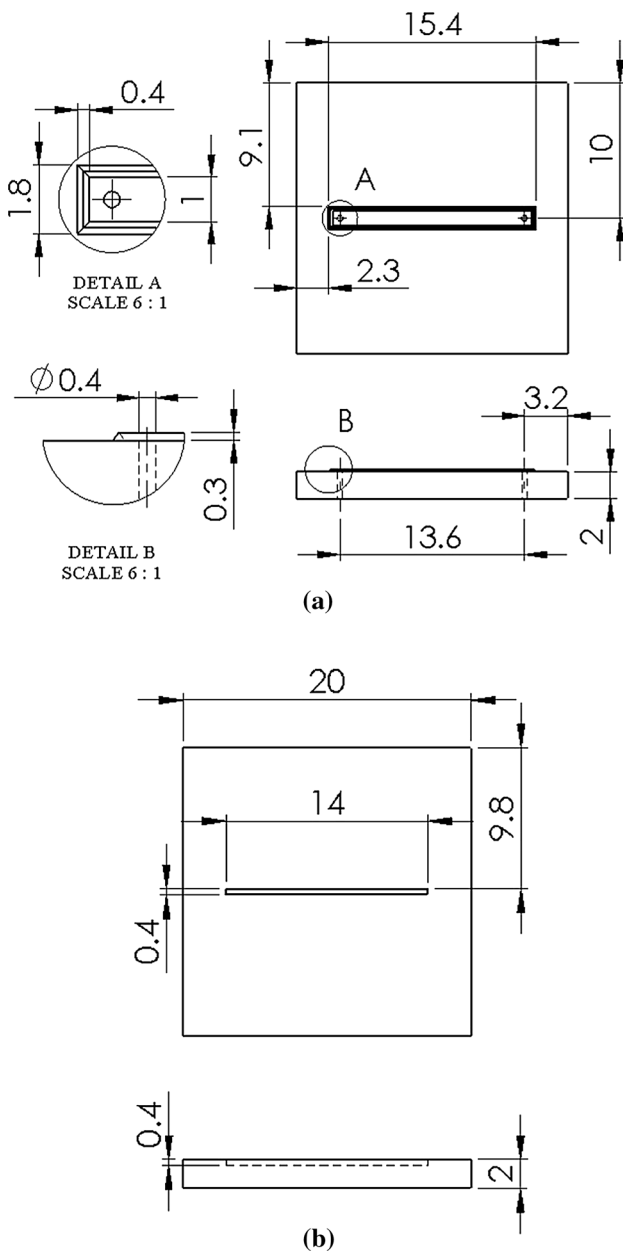**Fig. 3** Horn shape: **a** front view and **b** side view

(a)   **(b)**

(a)

(b)
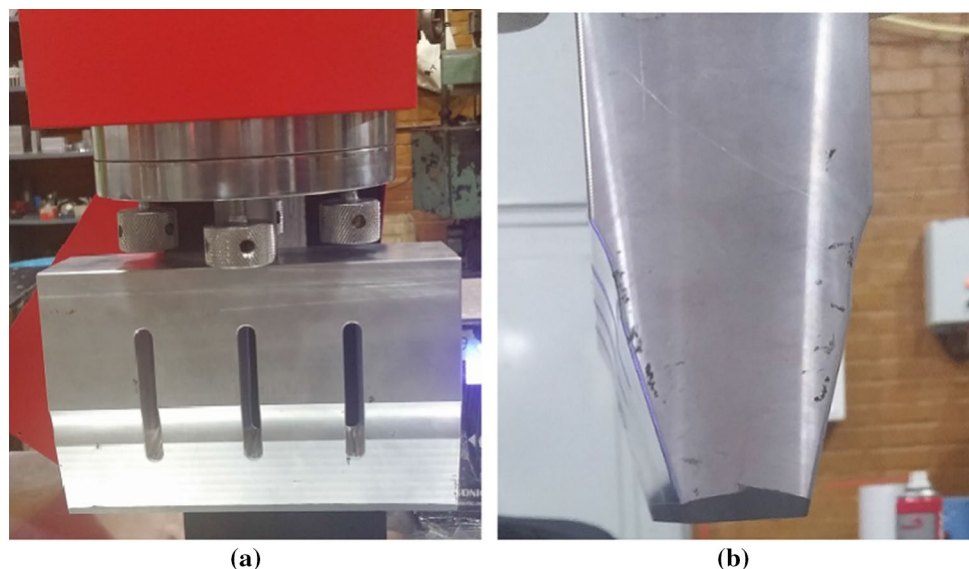
Fig. 4 Dimensions of the samples (units: mm), **a** top plate: EDs, inlet, and outlet and **b** bottom plate: micro-channel

(a)

(b)

Fig. 5 Picture of the microstructure components: **a** SEM image (with ×300 magnification) and **b** optical microscopic image (with ×100 magnification)

based on the orthogonal array concept which offers a systematic and efficient process. Taguchi Method is a statistical method that allows independent estimation of the response with a minimal number of experiments [29]. To determine the best design, it requires the use of strategically designed experiments. Taguchi method is performed as follows [30]:

1. Identifying the main functions and the process parameters to be evaluated
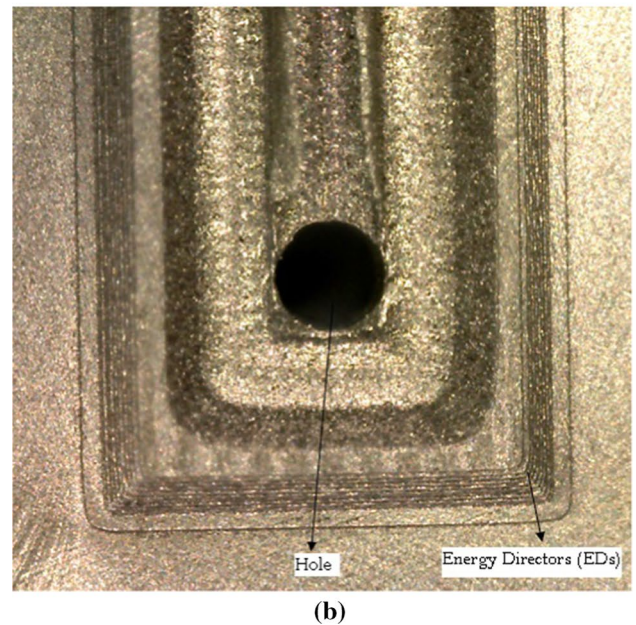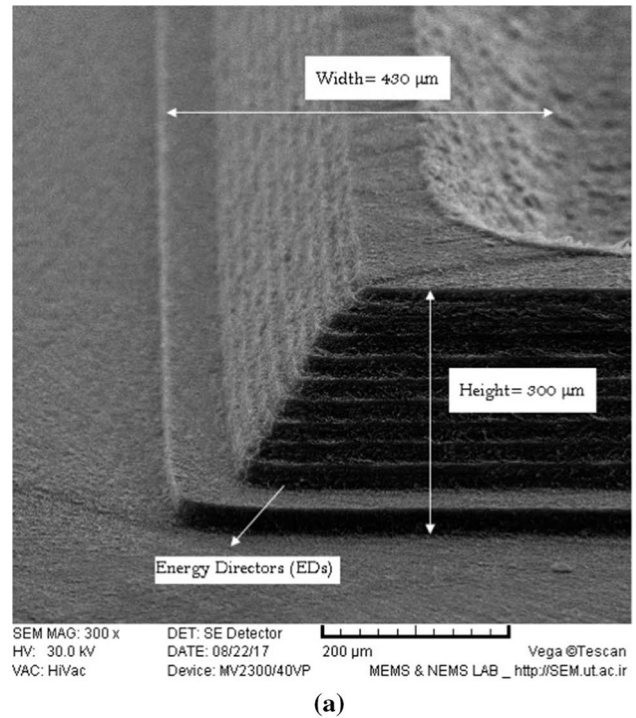2. Determination of the number of levels for the process parameters
3. Selecting the appropriate orthogonal array and assigning the process parameters to the orthogonal array and conducting the experiments accordingly
4. Studying the experimental results by analysis of the signal-to-noise (*S/N*) ratios to determine the optimum level of process parameters

5. Investigating the results by analysis of variance (ANOVA) to identify the significance level of the process parameters on the main function
6. Verifying the optimum process parameters through a confirmation experiment

In this study, target functions were defined as the maximum temperature created in the microstructure, heat zone area, and compressive-shear strength. The effective parameters on the target functions are the height of the energy directors (EDs), applied pressure, and loading time. According to the preliminary experiments, it was found that the height of the energy directors, applied pressure, and loading time parameters in the range of 300–600 mm, 2–3 bar, 0.1–0.3 s, remain a proper impact on the weld characteristics, respectively. Table 2 shows the quantity of each parameter on three levels based on Taguchi's method. An L_9 orthogonal array was selected to run the experiments. According to this orthogonal array, nine experiments were conducted to measure target functions that are given in Table 3.

Table 2 Effective parameters on the ultrasonic micro-welding process and related levels

Parameter	Level			Unit
	1	2	3	
Height of EDs	300	450	600	μm
Pressure	$2e^5$	$2.5e^5$	$3e^5$	Pa
Time	0.1	0.2	0.3	s

4 Experimental results analysis and discussion

Thermoplastic polymers have the visco-elastic property. In the ultrasonic micro-welding process, a compressive force with high-frequency is applied to weld the top and bottom plates to each other. According to input parameters, the applied cyclic load is:

$$F(t) = F_0 \times \mathrm{Sin}(w, t) \tag{1}$$

where F_0 represents the amplitude of the load, w indicates the angular frequency of loading, and t shows the time. The heat conductivity equation has the following form [31]:

$$C\rho \frac{\partial T}{\partial t} = k_x \frac{\partial^2 T}{\partial x^2} + k_y \frac{\partial^2 T}{\partial y^2} + k_z \frac{\partial^2 T}{\partial z^2} + Q \tag{2}$$

where C is the specific heat capacity at constant pressure, ρ is density, T is temperature, t is the welding time, k_x, k_y, k_z are the heat conductivity of materials in the three axial directions, Q is the dissipative function. Equation 2 shows that the total heat flow per unit length of the EDs is equal to the sum of the variation of the heat due to heat conductivity and the rate of heat release as a result of the dissipation of mechanical energy.

The total rate of supplied mechanical energy to the unit length of EDs is $\sigma(\partial\varepsilon/\partial t)$. A part of this energy is converted

Table 3 Conducted experiments based on the L9 orthogonal array and their results

A^1 (μm)	B^2 (Pa)	C^3 (s)	D^4 (K)	E^5 (mm^2)	F^6 (Pa)	G^7	H^8	I^9
300	$2e^5$	0.1	398	16.11	$4.17e^{13}$	− 51.9977	− 24.1419	272.403
300	$2.5e^5$	0.2	443	21.11	$4.55e^{13}$	− 52.9281	− 26.4898	273.160
300	$3e^5$	0.3	474	26.96	$5.15e^{13}$	− 53.5156	− 28.6144	274.236
450	$2e^5$	0.2	620	75.46	$1.42e^{13}$	− 55.8478	− 37.5543	263.046
450	$2.5e^5$	0.3	711	91.77	$1.27e^{13}$	− 57.0374	− 39.2540	262.076
450	$3e^5$	0.1	493	40.02	$2.21e^{13}$	− 53.8569	− 32.0455	266.888
600	$2e^5$	0.3	824	132.35	$5.8e^{12}$	− 58.3185	− 42.4345	255.269
600	$2.5e^5$	0.1	528	44.06	$1.39e^{13}$	− 54.4527	− 32.8809	262.860
600	$3e^5$	0.2	695	65.02	$1.28e^{13}$	− 56.8397	− 36.2609	262.144

[1]EDs Height

[2] Pressure

[3]Time

[4]Maximum temperature

[5]Welding area

[6]Maximum compressive-shear strength

[7]*S/N* Maximum temperature

[8]*S/N* Welding area

[9]*S/N* Maximum compressive-shear strength

to the heat with the rate Q, and the remaining part increases the potential energy [32]:

$$\sigma \frac{\partial \varepsilon}{\partial t} = Q + \left(\frac{\partial v}{\partial t}\right)_T \tag{3}$$

where V is the free energy of the unit volume. The presence of the term $\partial V / \partial t$ results in a change of temperature by no more than several degrees and, consequently, can be ignored. Consequently, the heat conductivity equation can be written in the following form

$$\frac{\partial T}{\partial t} = \alpha \frac{\partial^2 T}{\partial x^2} + \frac{\sigma}{c_P} \frac{\partial \varepsilon}{\partial t} \tag{4}$$

where α is the thermal diffusivity coefficient, equal to k/c_P. The solution of Eq. 4 with the appropriate initial and boundary conditions results in the temperature distribution along the length of the EDs.

4.1 Temperature distribution

The rapid heating of plastics in ultrasonic welding takes place by the same mechanism as in any type of cyclic deformation after reaching the critical temperature. It has been assumed that the hysteresis losses created in the energy directors are the heat source for the ultrasonic welding of the PMMA microstructures. Therefore, energy directors cause two plates of PMMA to be welded to each other. Energy directors are known as energy concentrators. They must have proper mechanical design and properties that can be melted under oscillating forces during process for bonding the two plates. Analysis of the temperature distribution during the ultrasonic welding process is necessary to minimize the amount of deformation in the microstructures by selecting the optimal level of the parameters. Figures 6 and 7 show the distribution of temperature in the PMMA plates and energy directors.

The increase in the local temperature at the location of EDs is due to two factors. One of these factors is the damping of oscillations due to internal friction between polymer plates, which depends on the damping properties of the PMMA polymer. The other factor is the creation of friction between the polymer grains. Both factors cause temperature increase in the PMMA above the glass transition temperature (378 K) and the melting point temperature (393 K). The maximum amount of generated temperature during the welding process in the energy directors and PMMA plates is given in Table 3.

4.2 Welding area

Investigation of the welding affected area is important to analyze the amount of deformation of the micro-channel path during the welding process. The welding areas were examined on nine samples according to the L_9 array (Table 3) by an optical microscope with a magnification of ×20. The results are shown in Fig. 8. The melted and affected areas by the welding process are given in Table 3. Comparison of the welding area (Fig. 8, resulted from the experiments) with max. temperature (Fig. 7, Table 3, resulted from the simulations) shows that the simulation results have a good accordance with the experimental results.

4.3 Compressive-shear strength

The compressive-shear strength test was performed on the micro-welded specimens to check the strength of the micro-weld by Instron 4208 machine. The above clamp of the machine is moveable and the other one is fixed (Fig. 9). As shown in this figure, an aluminum fixture was used to prevent the unwanted movement of the specimen during the test. The welded samples located between the clamps were subjected to pressure with 0.5 mm/min compressive loading rate. For achieving the compressive-shear strength, the parallel forces are applied to the two plates of the specimens. The obtained amount of the compressive-shear strength up to the strain value of 0.04 has been shown for the samples in Fig. 10.

5 Process optimization by using Taguchi method

5.1 Analysis of the signal-to-noise ratio

In the Taguchi method, the optimal level of process parameters is determined using the signal-to-noise ratio (S/N) analysis. In this method, there are several efficiencies such as "less is better" (LB), "nominal value is better" (NB), and "higher is better" (HB) [33]. The response function "LB" was selected as the optimal efficiency of the process, because of the affected area and generated maximum temperature during the process should be as low as possible. On the other hand, the maximum amount of compressive-shear strength of the samples should be high. Therefore, "HB" was selected as the process optimal efficiency for this response function. The S/N ratio was defined with a "loss" logarithmic function. This ratio is expressed as Eqs. 5 and 6 for "LB" and "HB" modes, respectively.

$$(S/N)_S = -10 \log \left(\frac{1}{n} \sum y_i^2\right) \tag{5}$$

$$(S/N)_L = -10 \log \left(\frac{1}{n} \sum \frac{1}{y_i^2}\right) \tag{6}$$

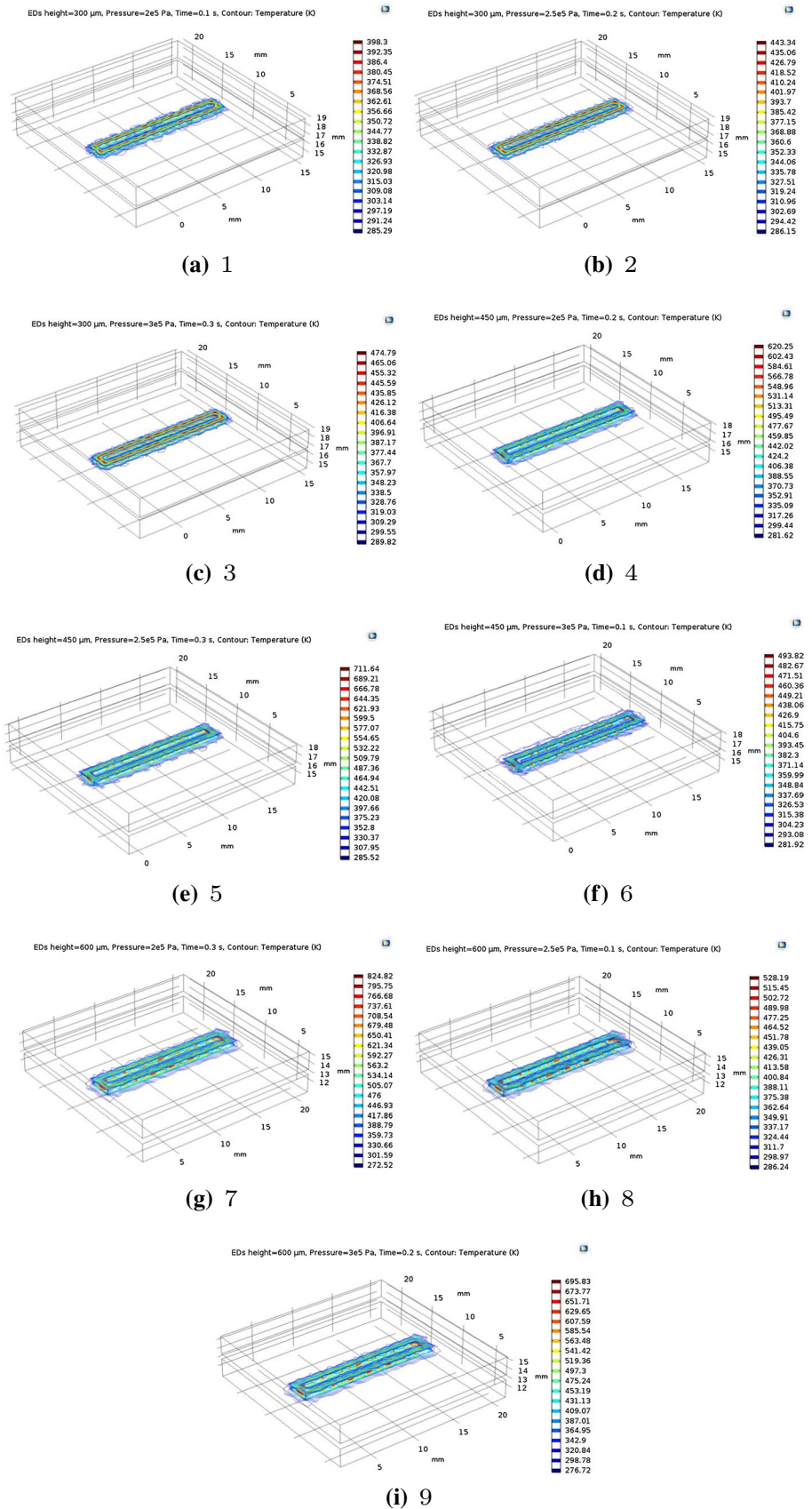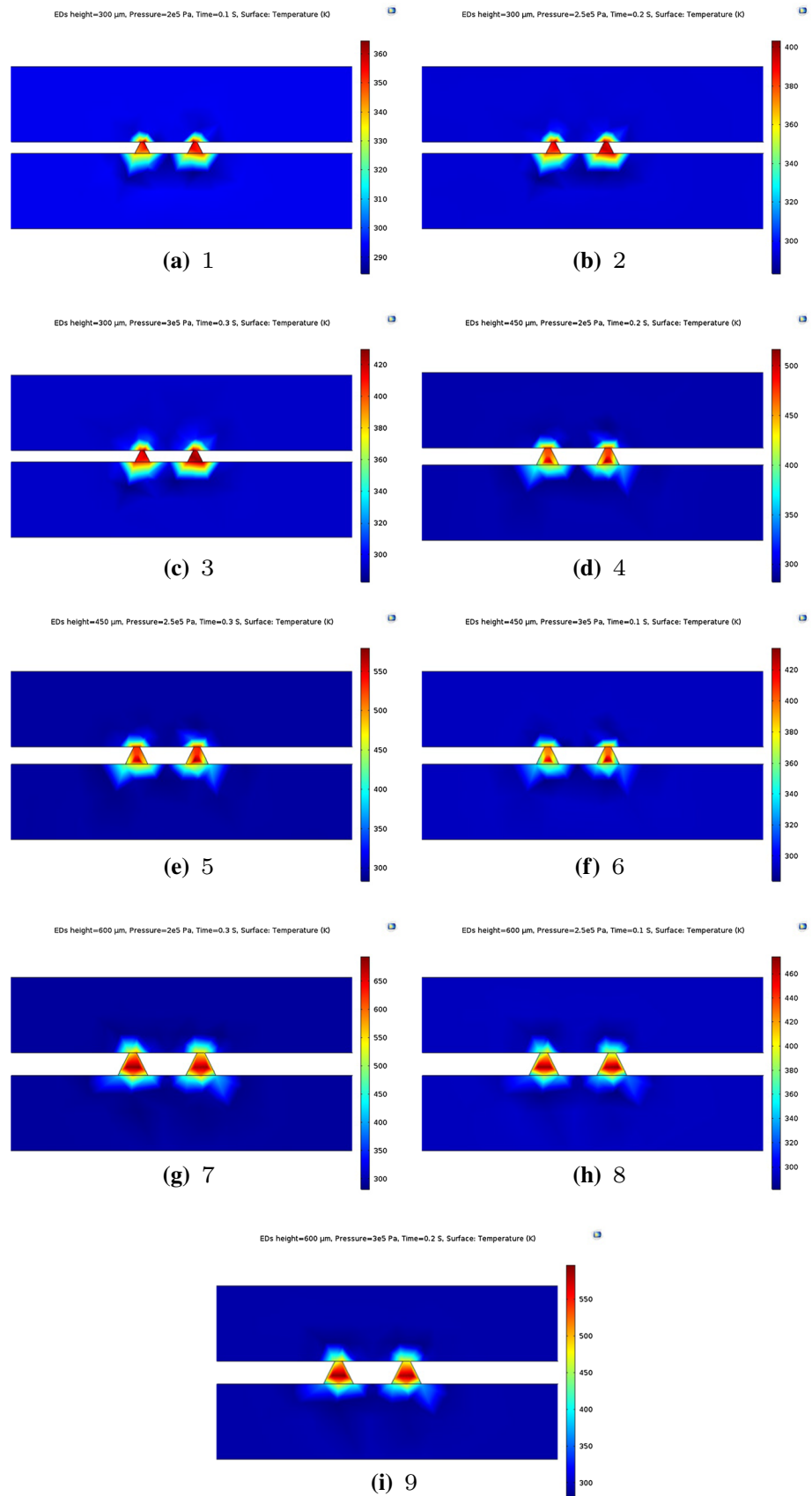**Fig. 6** Temperature distribution during the ultrasonic micro-welding process

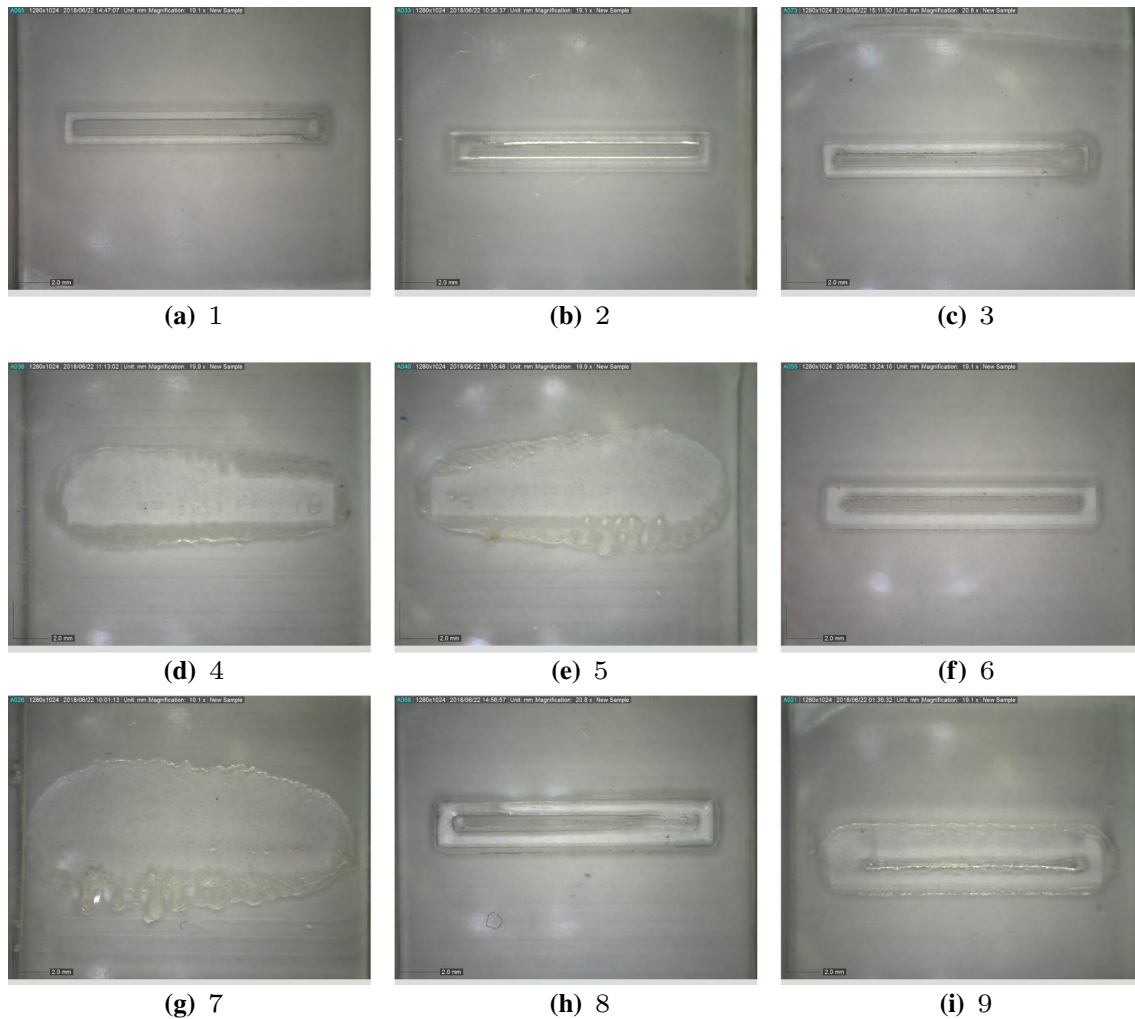**Fig. 7** Temperature distribution on the cross-sectional view of the PMMA plates and EDs

Fig. 8 Images of the affected areas by the ultrasonic micro-welding

where y_i is the answer to the i-th test, n represents the number of repetitions of each test. Regardless of the selected efficiency level, the higher the S/N ratio is better. The values of the S/N ratio are given in Table 3 for the L_9 orthogonal array. Figure 11 shows the average values of signal-to-noise ratios for different target functions versus specified different levels for the parameters of the height of EDs, affected area, and maximum generated temperature during the welding process. Optimal levels of parameters of the ultrasonic micro-welding process to create the minimum temperature during the process, minimum affected area, and maximum amount of the tolerable compressive-shear strength of welded sheets

by studying the diagrams of signal-to-noise (Fig. 11) are as follows: height of the EDs of 300 μm, the applied pressure of $3e^5$ Pa and the loading time of 0.1 s.

5.2 Analysis of variance

The relative importance of the process parameters on the welding process performance was studied to determine the optimum combinations of the process parameters by using the analysis of variance (ANOVA) [34]. In this analysis method, the sum of the total squares (SS_{Total}) shows the total scatter between the differences of the signal-to-noise

Fig. 9 Compressive-shear strength testing setup: **a** before testing, **b** during the test, and **c** graph of the applied force in terms of strain
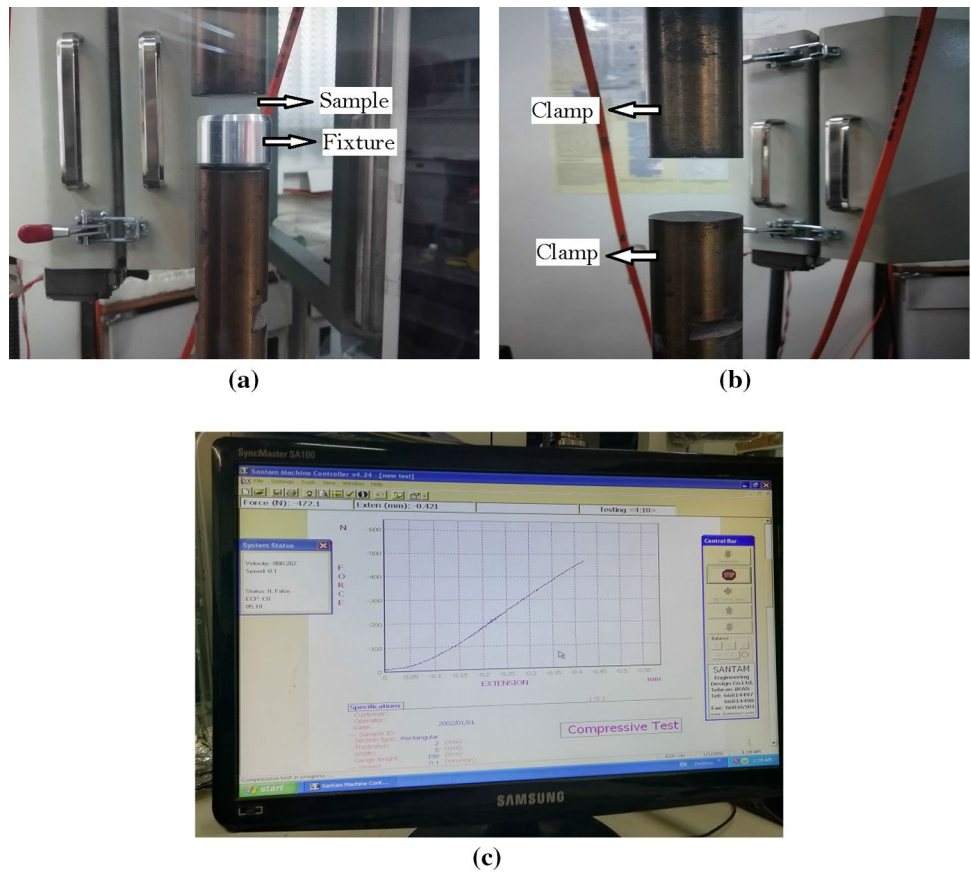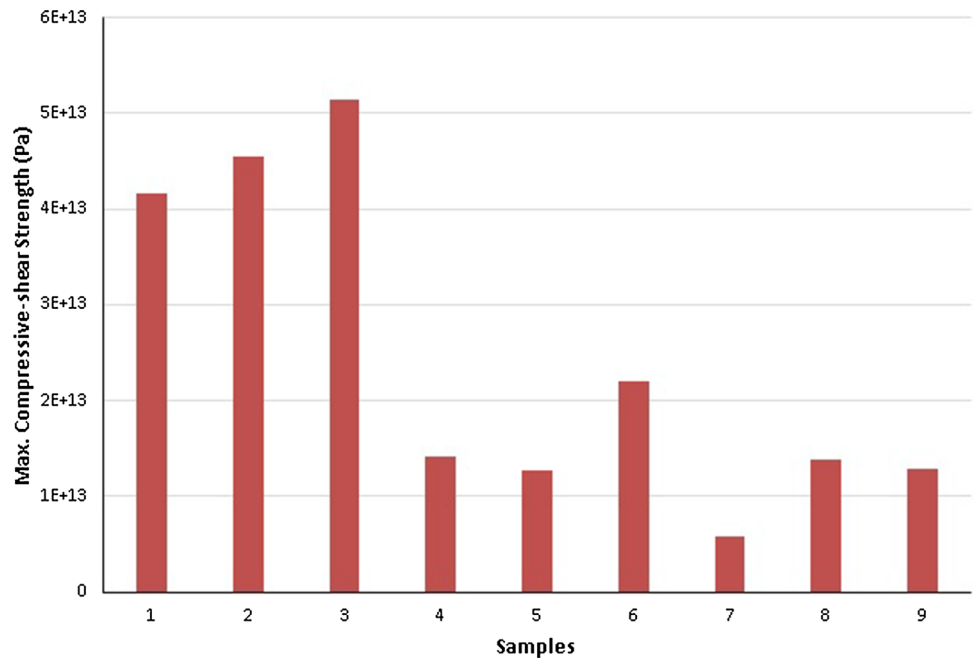

(a)

(b)

(c)

Fig. 10 Compressive-shear strength of the welded samples

ratio of each tested sample with the total average of the signal-to-noise ratios. This dispersion can be divided into two parts. First, the distribution between the groups is obtained from the difference between the average of each group and the total average, which shows the difference between the groups (the sum of squares for each parameter (SS_A)). The second part is the intragroup scattering, which shows the difference between the signal-to-noise ratio of each sample and the average of its group (the sum of squares of the error (SS_E)). Therefore, the total distribution can be written as follows:

$$SS_{Total} = SS_A + SS_E. \tag{7}$$

If we divide the dispersion between the groups by its degree of freedom, we will get the variance between the groups (main square average (MS_A)). We use F fraction to reject or accept the hypothesis zero. Also, if we divide the intragroup scatter by its degree of freedom, we get the intragroup variance (main square error (MS_E)), which we put in the denominator of the fraction F. Therefore, the fraction F is as follows:

$$F = \frac{MS_A}{MS_E}. \tag{8}$$

The results obtained from ANOVA of the *S/N* ratios are shown in Table 4. Greater F (F_T, F_A, F_S) value for a parameter determines the higher impact of the parameter on the max. temperature in the welding process, welding area, and max. compressive-shear strength, respectively. Considering the ANOVA results given in Table 4, the process parameters can be ranked in terms of their impact.

5.3 Confirmation Test

Proof of the process performance improvement using optimal levels of the process parameters is the last step of the Taguchi method. The estimated *S/N* ratio (η_{opt}) using the optimum level of the process parameters is shown by Eq. 9.

Fig. 11 Average values of signal-to-noise ratios for different target ▶ functions: **a** maximum created temperature, **b** affected area by the welding, and **c** maximum tolerable compressive-shear strength, versus specified different levels for the process parameters

$$\eta_{opt} = \eta_m + \sum_{i=1}^{p} \left(\bar{\eta}_i - \eta_m \right) \tag{9}$$

where η_m is the average value of the obtained total signal-to-noise ratios for each studied response function, p is the number of process parameters, and $\bar{\eta}_i$ is the average value of the signal-to-noise ratio of the optimal level for each parameter. The results of the confirmation test are shown in Table 5. The amount of max. temperature, welding area, and max. compressive-shear strength obtained for optimal levels of the process parameters is 398 K, 15.17 mm^2, and $5.2e^{13}$ Pa, respectively.

6 Conclusion

In this paper, the effects of the ultrasonic micro-welding process parameters (height of the EDs, applied pressure, and loading time) were studied by using the Taguchi method. The effects of change in these parameters on the temperature distribution during the micro-welding process, the affected area by welding, and the maximum value of the tolerable compressive-shear strength by the micro-welded samples were analyzed. The EDs height of 300 μm, applied pressure of 3 bar, and process time of 0.1 s lead to the optimum ultrasonic micro-welding process performance. The order of importance of the process parameters was specified by using the analysis of variance (ANOVA) of the *S/N* ratios. According to the confirmation experiment, the max. temperature during the process, the welding area, and the max. compressive-shear strength for the optimal levels of the process parameters are 398 K, 15.17 mm^2, $5.2e^{13}$ Pa, respectively.
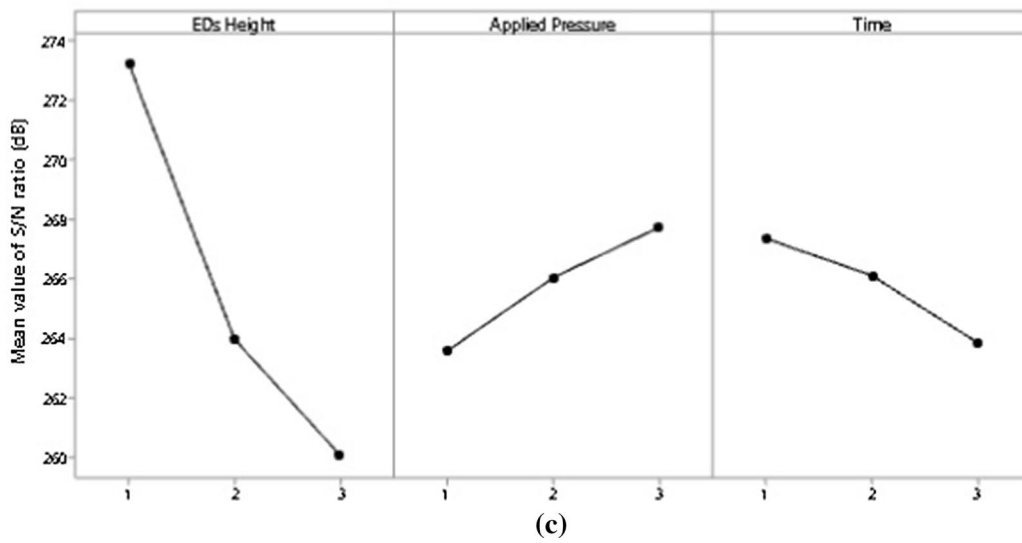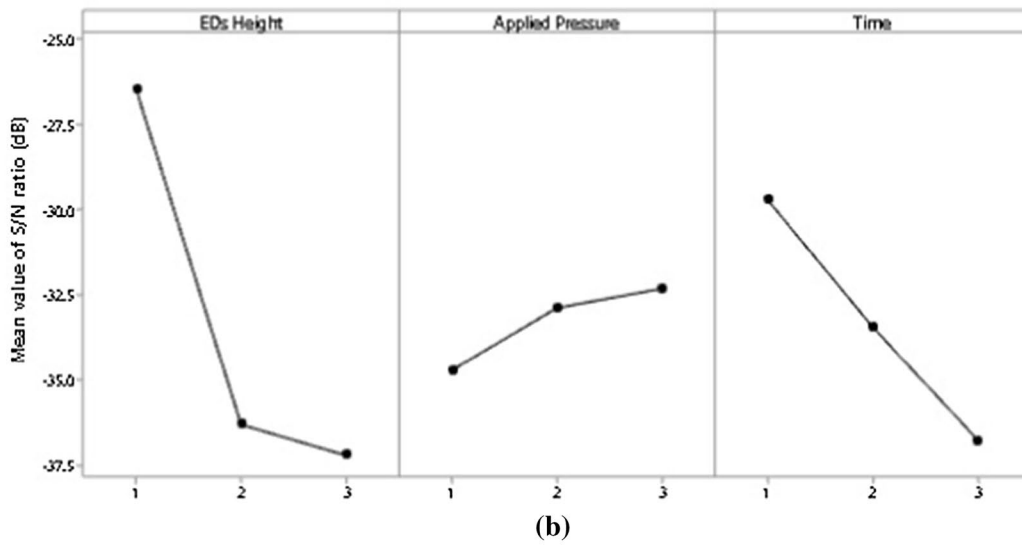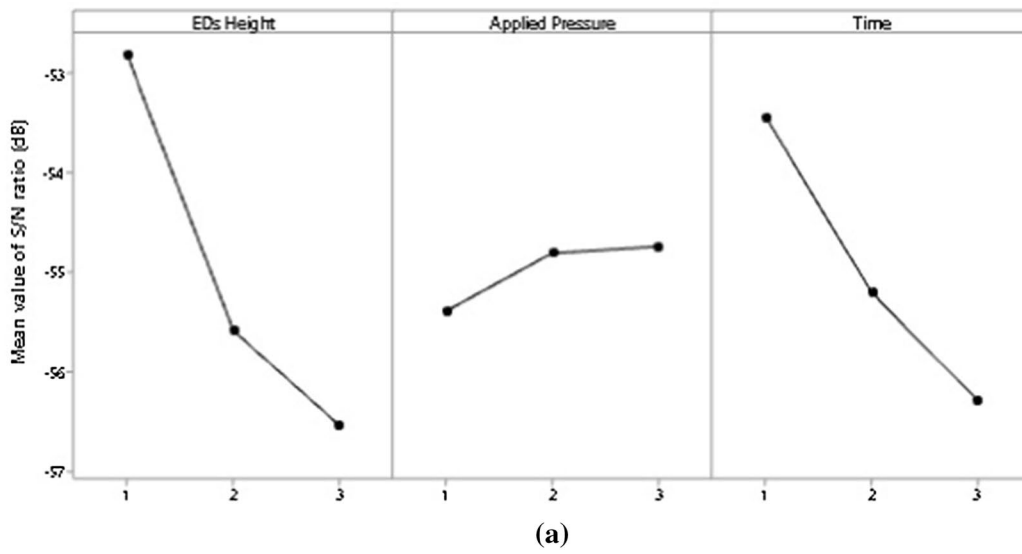
(a)

(b)

(c)

Table 4 Analysis of variance (ANOVA) results

Source	SS_T	F_T	SS_A	F_A	SS_S	F_S
EDs height	22.431	31.152	214.363	333.899	274.698	66.128
Pressure	0.767	1.063	9.466	14.745	26.52	6.384
Time	12.458	17.302	75.236	18.809	19.11	4.6
Error	0.720		0.642		4.154	
Total	36.378		299.709		324.482	

Table 5 Results of the confirmation test

Response functions	Signal-to-noise ratio (dB)	
	Predicted *S/N* ratios	Experiment *S/N* ratios
Max. temperature	− 51.03	− 51.99
Welding area	− 21.81	− 24.14
Max. compressive-shear strength	276.83	274.236

References

1. Tahmasebipour M, Modarres M (2018) Simulation of a highly sensitive piezoresistive differential pressure microsensor. Iran J Electr Electron Eng 14(4):374–381
2. Tahmasebipour M, Vafaie A (2017) A highly sensitive three axis piezoelectric microaccelerometer for high bandwidth applications. Micro Nanosyst 9(2):111–120
3. Tahmasebipour M, Vafaie A (2020) A novel single axis capacitive MEMS accelerometer with double-sided suspension beams fabricated using μWEDM. Sens Actuators A 309:112003
4. Vafaie A, Tahmasebipour M, Tahmasebipour Y (2019) A novel capacitive micro-accelerometer made of steel using micro wire electrical discharge machining method. J Micromech Microeng 29(12):125018
5. Tahmasebipour M, Sangchap M (2019) A novel high performance integrated two-axis inchworm piezoelectric motor. Smart Mater Struct 29(1):015034
6. Sangchap M, Mohammad T, Younes T (2020) A linear inchworm piezomotor with a new configuration: design considerations, fabrication and characterization. Iran J Sci Technol Trans Mech Eng 46:1–12
7. Paknahad AA, Tahmasebipour M (2019) An electromagnetic micro-actuator with PDMS-Fe3O4 nanocomposite magnetic membrane. Microelectron Eng 216:111031
8. Tahmasebipour M, Paknahad AA (2019) Unidirectional and bidirectional valveless electromagnetic micropump with PDMS-Fe3O4 nanocomposite magnetic membrane. J Micromech Microeng 29(7):075014
9. Koesdjojo MT, Koch CR, Remcho VT (2009) Technique for microfabrication of polymeric-based microchips from an SU-8 master with temperature-assisted vaporized organic solvent bonding. Anal Chem 81(4):1652–1659
10. Torunbalci MM, Alper SE, Akin T (2015) Wafer level hermetic sealing of MEMS devices with vertical feedthroughs using anodic bonding. Sens Actuators A 224:169–176
11. Petersen K, Barth P, Poydock J, Brown J, Mallon J, Bryzek J (1988) Silicon fusion bonding for pressure sensors. In: IEEE technical digest on solid-state sensor and actuator workshop. IEEE, pp 144–147
12. Barako MT, Gao Y, Won Y, Marconnet AM, Asheghi M, Goodson KE (2014) Reactive metal bonding of carbon nanotube arrays for thermal interface applications. IEEE Trans Compon Packag Manuf Technol 4(12):1906–1913
13. Ng SH, Wang ZF, De Rooij NF (2009) Microfluidic connectors by ultrasonic welding. Microelectron Eng 86(4–6):1354–1357
14. Fukumoto S, Fujiwara K, Toji S, Yamamoto A (2008) Small-scale resistance spot welding of austenitic stainless steels. Mater Sci Eng A 492(1–2):243–249
15. Troughton MJ (2008) Handbook of plastics joining: a practical guide. William Andrew, Norwich
16. Chen K, Zhang Y, Wang H (2017) Effect of acoustic softening on the thermal–mechanical process of ultrasonic welding. Ultrasonics 75:9–21
17. Truckenmüller R, Ahrens R, Cheng Y, Fischer G, Saile V (2006) An ultrasonic welding based process for building up a new class of inert fluidic microsensors and-actuators from polymers. Sens Actuators A 132(1):385–392
18. Chen C, Yan L, Kong ES-W, Zhang Y (2006) Ultrasonic nanowelding of carbon nanotubes to metal electrodes. Nanotechnology 17(9):2192
19. Grund T, Cuntz T, Kohl M (2008) Batch fabrication of polymer microsystems with shape memory microactuators. In: 2008 IEEE 21st international conference on micro electro mechanical systems. IEEE, pp 423–426
20. Min J, Park J-H, Yoon HH, Choy YB (2008) Ultrasonic welding method to fabricate polymer microstructure encapsulating protein with minimum damage. Macromol Res 16(6):570–573
21. Luo Y, Zhang Z, Wang X, Zheng Y (2010) Ultrasonic bonding for thermoplastic microfluidic devices without energy director. Microelectron Eng 87(11):2429–2436
22. Michaeli W, Kamps T, Hopmann C (2011) Manufacturing of polymer micro parts by ultrasonic plasticization and direct injection. Microsyst Technol 17(2):243–249
23. van Oordt T, Barb Y, Smetana J, Zengerle R, von Stetten F (2013) Miniature stick-packaging-an industrial technology for pre-storage and release of reagents in lab-on-a-chip systems. Lab Chip 13(15):2888–2892
24. Ali U, Karim KJBA, Buang NA (2015) A review of the properties and applications of poly (methyl methacrylate) (PMMA). Polym Rev 55(4):678–705
25. Mott PH, Dorgan JR, Roland CM (2008) The bulk modulus and Poisson's ratio of "incompressible" materials. J Sound Vib 312(4–5):572–575
26. Tahmasebipour G, Ahmadi V, Abdullah A, Hojjat Y (2009) Fabrication of STM tungsten nanotip by electrochemical etching method. Int J Nanosci 8(03):305–310
27. Mohsin I, He K, Li Z, Zhang F, Ruxu D (2020) Optimization of the polishing efficiency and torque by using Taguchi method and ANOVA in robotic polishing. Appl Sci 10(3):824

28. Manni A, Saviano G, Bonelli MG (2021) Optimization of the ANNs predictive capability using the Taguchi approach: a case study. Mathematics 9(7):766

29. Ginting E, Tambunan MM (2018) Selection of optimal factor level from process parameters in palm oil industry. IOP Conf Ser Mater Sci Eng 288(1):012056

30. Tahmasebipour Gh, Hojjat Y, Ahmadi V, Abdullah A (2009) Optimization of STM/FIM nanotip aspect ratio based on the Taguchi method. Int J Adv Manuf Technol 44(1):80–90

31. Wang X, Yan J, Li R, Yang S (2006) FEM investigation of the temperature field of energy director during ultrasonic welding of PEEK composites. J Thermoplast Compos Mater 19(5):593–607

32. Han W, Liu J, Chong D, Yan J (2016) Analysis of heat generation characteristics in ultrasonic welding of plastics under low amplitude conditions. J Polym Eng 36(4):413–419

33. Tahmasebipour Gh, Hojjat Y, Ahmadi V, Abdullah A (2009) Effect of fabrication process parameters on the apex-radius of STM tungsten nanotip. Scanning: J Scanning Microsc 31(2):65–74

34. Phadke MS (1989) Quality engineering using robust design. PTR Prentice-Hall. Inc., Englewood Cliffs